

Article

Characterization of a New Glyoxal Oxidase from the Thermophilic Fungus *Myceliophthora thermophila* M77: Hydrogen Peroxide Production Retained in 5-Hydroxymethylfurfural Oxidation

Marco Antonio Seiki Kadowaki ^{1,2}, Mariana Ortiz de Godoy ^{1,2}, Patricia Suemy Kumagai ¹ , Antonio José da Costa-Filho ³, Andrew Mort ², Rolf Alexander Prade ^{2,*} and Igor Polikarpov ^{1,*} 

¹ São Carlos Institute of Physics, University of São Paulo, Av. Trabalhador São-Carlense, 400, São Carlos 13566-590, Brazil; marcocadowaki@gmail.com (M.A.S.K.); marianaort@gmail.com (M.O.d.G.); patysuemy@gmail.com (P.S.K.)

² Departments of Biochemistry & Molecular Biology and Microbiology & Molecular Genetics, Oklahoma State University, Stillwater, OK 74078, USA; andrew.mort@okstate.edu

³ Department of Physics, Ribeirão Preto School of Philosophy, Sciences and Literature, University of São Paulo, Ribeirão Preto BR-14040901, Brazil; ajcosta@usp.br

* Correspondence: rolf.prade@okstate.edu (R.A.P.); ipolikarpov@ifsc.usp.br (I.P.); Tel.: +1-405-744-7522 (R.A.P.); +55-16-3373-8088 (I.P.)

Received: 2 October 2018; Accepted: 16 October 2018; Published: 19 October 2018



Abstract: *Myceliophthora thermophyla* is a thermophilic industrially relevant fungus that secretes an assortment of hydrolytic and oxidative enzymes for lignocellulose degradation. Among them is glyoxal oxidase (*MtGLOx*), an extracellular oxidoreductase that oxidizes several aldehydes and α -hydroxy carbonyl substrates coupled to the reduction of O_2 to H_2O_2 . This copper metalloprotein belongs to a class of enzymes called radical copper oxidases (CRO) and to the “auxiliary activities” subfamily AA5_1 that is based on the Carbohydrate-Active enZYmes (CAZy) database. Only a few members of this family have been characterized to date. Here, we report the recombinant production, characterization, and structure–function analysis of *MtGLOx*. Electron Paramagnetic Resonance (EPR) spectroscopy confirmed *MtGLOx* to be a radical-coupled copper complex and small angle X-ray scattering (SAXS) revealed an extended spatial arrangement of the catalytic and four N-terminal WSC domains. Furthermore, we demonstrate that methylglyoxal and 5-hydroxymethylfurfural (HMF), a fermentation inhibitor, are substrates for the enzyme.

Keywords: *Myceliophthora*; glyoxal oxidase; 5-hydroxymethylfurfural

1. Introduction

Waste plant biomass could be a massive resource for biofuels and commodity chemicals. Two-thirds of a typical biomass is composed of polysaccharides. The predominant polysaccharide is cellulose, a $\beta(1,4)$ glucan followed by hemicelluloses a group of $\beta(1,4)$ linked polysaccharides that interact with cellulose but can be solubilized in strong alkali [1,2]. Another abundant biomass components is lignin, a polyphenolic complex, which forms an insoluble network that confers rigidity to plant cell walls [3].

Natural recycling of biomass entails decomposition of the polysaccharides into simple sugars by microorganisms that use them as a carbon source for growth. Many microorganisms produce a wide variety of hydrolytic enzymes to degrade the polymers. These enzymes can be used in some industrial settings to extract sugars from biomass, which can then be converted into useful

commodities, such as fuels (typically ethanol and biodiesel), organic acids (citric and succinic acid), and other bio commodities with high aggregate value. The barriers for biomass conversion to valuable products are the high cost of the enzymatic cocktails needed to break down the polysaccharides and the generation of inhibitory compounds, such as furfural and 5-hydroxymethylfurfural (HMF), which can inhibit enzymatic action or microbial growth in fermentation processes [4,5]. Furfural and 5-hydroxymethylfurfural (HMF) are derived from pentoses and hexoses, respectively, via dehydration during, for example, dilute acid pretreatment [6] or catalytic pyrolysis of lignocellulosic biomass [7]. These chemicals can follow different oxidation/reduction pathways for the production of renewable building blocks for the polymer industry [8]. 2,5-diformylfuran (DFF), a direct product from HMF oxidation, is applied for polymer resin synthesis [9]. 2,5-furandicarboxylic acid (FDCA), originated from two oxidation steps from DFF to 2,5-formylfurancarboxylic acid (FFCA) and FDCA, co-polymerize and produce a polyester with plastic properties [10] and 2-methylfuran, a product of furfural hydrogenolysis, can react with ketones and produce branched-chain liquid hydrocarbons with fuel properties [7,11].

A variety of microorganisms produce an arsenal of enzymes to obtain nutrients from biomass. Not all degrade biomass in the same way. Some use predominantly hydrolytic mechanisms for breaking down glycosidic bonds, while others utilize a combination of hydrolytic and oxidative mechanisms. Based on genome and secretome analysis, the thermophilic fungus, *Myceliophthora thermophila*, isolated from soil and natural composts with high temperatures and humidity [12,13], is an oxidative enzyme producer. Its enzymes are thermo tolerant, which is a desirable characteristic in the biotechnological field.

The classical hydrolytic mechanism employs enzymes that hydrolyze the glycosidic bonds through a general acid/base mechanism [14]. On the other hand, as predicted in 1974, oxidoreductive enzymes that directly oxidize glycans and lignin have been discovered, confirming the role of oxidation reactions in the breakdown of biomass components [15]. The so-called oxizymes play a fundamental role as auxiliary enzymes enhancing cellulase action and cellulose accessibility [16,17]. Oxizymes can also target lignin providing greater access of cellulases to cellulose. Some of these enzymes generate hydrogen peroxide, as a by-product that can feed lignin peroxidases for depolymerization of lignin, or, can generate hydroxyl radicals by Fenton chemistry that can directly attack the biomass structure [18,19].

Glyoxal oxidase (GLOx) (E.C. 1.2.3.15) is an extracellular copper metalloenzyme that belongs to a class of enzymes called radical copper oxidases (CRO) [20,21]. Based on the Carbohydrate-Active enZymes database (CAZy), these enzymes fall into the “auxiliary activities” subfamily AA5_1 in the CAZy database [22,23]. Family AA5 also includes a second subfamily, AA5_2, containing galactose and alcohol oxidases. GLOx couples the two-electron oxidation of aldehydes to carboxylic acids to the reduction of O₂ to H₂O₂ [21,24,25], α -Hydroxy carbonyl and α -diol substrates can also be oxidized in two steps to carboxylic acids. Previous reports on the enzymatic activity of GLOxes from *Phanerochaete chrysosporium* [26] and *Pycnoporus cinnabarinus* [27] indicate that glyoxal and methylglyoxal are the best substrates for the enzymes. Both aldehydes are recognized as products of glucose degradation through a combination of retroaldol condensation and auto-oxidation and are found in ligninolytic cultures [28,29]. Another reported substrate that is oxidized by GLOx is glycerol, formed in bulk during biodiesel production [25]. Experimental evidence suggests that GLOxes need to be activated by other enzymes such as lignin peroxidases and can enhance ligninolytic activity of white-rot fungi in biomass degradation [26,29,30]. Glycoaldehydes, products from lignin degradation and inhibitors of bioethanol fermentation, have been suggested to be GLOx substrates [31]. Thus, GLOx could play a detoxifying role in the inhibitory aldehydes [21]. Spectroscopic and sequence analysis show that GLOx, CgrAlcOx (Alcohol oxidase from *Colletotrichum graminicola*), and galactose-6-oxidase share similar active sites containing a phenoxy radical-copper motif [20,32,33]. This copper ion is coordinated by two histidine residues and a tyrosine, which is cross-linked to a cysteine residue by an unusual thioester bond. These residues are conserved in GLOxes, CgrAlcOx, and galactose-6-oxidases [27,31,32].

The central physiological function of GLOx remains unknown, but experimental reports reveal that the enzyme is important for hyphal tip development and pathogenicity [34,35]. Moreover, some GLOxes are linked to the cell Wall Stress-responsive Component (WSC) domain that is predicted to be a cell-wall and membrane protein in yeast and fungi associated with cell wall integrity and stress responses [36,37]. Only three catalytic domains of GLOx enzymes from *Phanaerochaete chrysosporium*, *Ustilago maydis*, and *Pycnoporus cinnabarinus* fungi have been studied biochemically to date [26,27,34,38], but none were associated with such WSC domains. In the present study, we report the structural and functional characterization of a multidomain glyoxal oxidase from the thermo tolerant *Myceliophthora thermophila* M77 and show that 5-hydroxymethylfurfural as a new described substrate for this enzyme, demonstrating its potential in green enzymatic synthesis.

2. Results and Discussion

2.1. Comparative Analysis of MtGLOx with Other Copper Radical Oxidases

Complete AA5_1 glyoxal oxidase genes are present in the genomes of various fungi (mainly Basidiomycete and also some Ascomycetes) and several plant genomes. The three-dimensional (3D) structure of the MtGLOx catalytic domain has not yet been solved by experimental methods but the sequence shares 25% sequence identity with the galactose oxidases from *Streptomyces lividans* (PDBid: 4UNM) [39] and *Fusarium graminearum* (PDBid: 1GOF) and alcohol oxidase from *Colletotrichum graminicola* (PDBid: 5C92) [33] indicating a similar fold, albeit with possible different substrate specificities.

Phylogenetic analysis of 47 predicted AA5_1 domains of GLOx enzymes shows that MtGLOx is grouped within a distinct cluster that does not include the characterized GLOx from *P. chrysosporium*, *P. cinnabarinus*, and *U. maydis* (Figure 1). Interestingly, all WSC associated enzymes were clustered together, based on the alignment of just AA5_1 domains (Figure 1). Fungal glyoxal oxidase AA5_1 genes analyzed lack a WSC domain or have one to six of them, followed by a linker that connects with the classical C-terminal copper-radical oxidase catalytic domain (Figure 1). The *M. thermophila* glyoxal oxidase AA5 has four WSC domains. On the other hand, GLOxes from higher plants, *Arabidopsis thaliana*, *Oryza sativa*, *Theobroma cacao*, and *Zea mays* all have just the catalytic domain as do the characterized enzymes from *P. chrysosporium*, *U. maydis*, and *P. cinnabarinus*. Four GLOxes from the Ascomycete group, closely related to representatives from the plant group, have chitin-binding domains (ChtBD) instead of WSC domains. The WSC domain is considered as a putative carbohydrate binding domain that contains up to eight conserved cysteines involved into disulfides bridges formation and is crucial for fungal adaptation [40]. Two WSC domains which putatively mediate interactions with glucan chains have been previously identified in *Trichodema harzianum* β -1,3-exoglucanase [41]. WSC proteins from *A. nidulans* involved with hypo-osmotic and acidic pH stress tolerance presents extra regions: a potentially glycosylated serine/threonine-rich, transmembrane, and highly charged C-terminal cytoplasmic region besides WSC domain [37]. Moreover, the WSC domains are required for Wsc1 protein clustering that signalize stress conditions [42]. These occurrences and extra associations are suggested to be correlated with the metabolism type of the diverse fungi [43]. The relationship between fungal peroxidases and GLOxes are also been described [21] and it suggests a coupled reaction that is associated with lignin degradation. However, *M. thermophila* do not codify or secrete this class of peroxidases [12]. Thus, MtGLOx could work as a H₂O₂ provider to other oxidative enzymes, such as lytic polysaccharide monoxygenases (LPMO) [44] or used to attack putative pathogens [45].

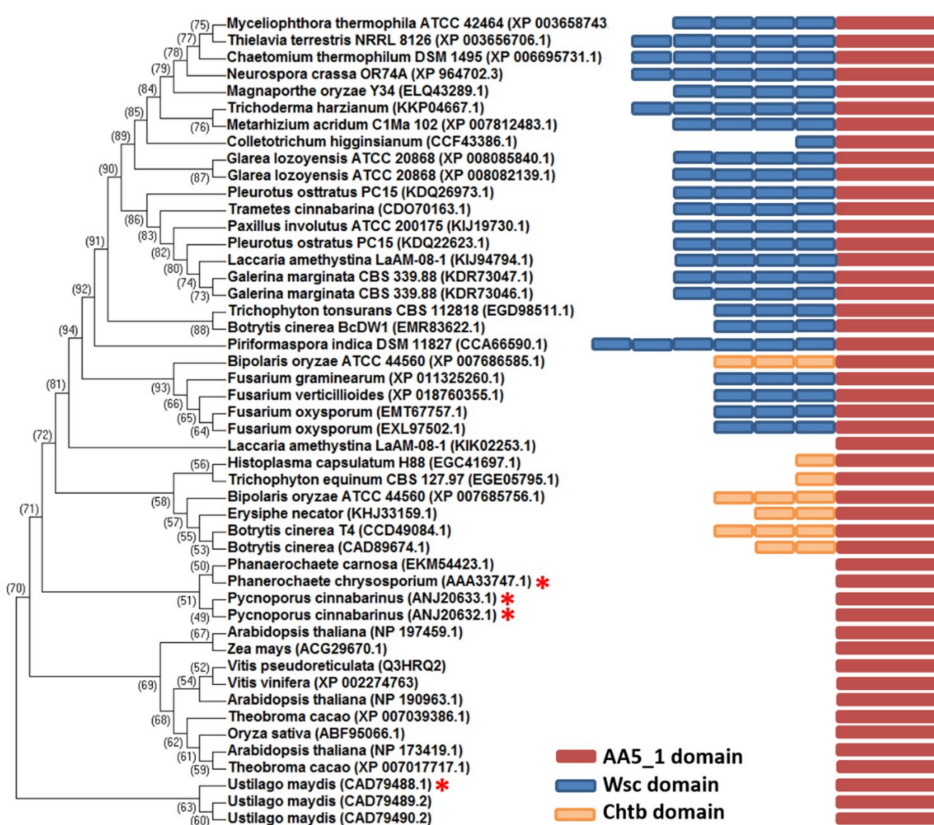


Figure 1. Domain organization of glyoxal oxidases. Phylogenetic tree of predicted AA5 domains of glyoxal oxidase (GLOx) enzymes. The N-terminal Wall Stress-responsive Component (WSC)/Chtb domains were removed to avoid alignment bias. Muscle alignment and tree constructed using MEGA are shown. The GLOx domains were annotated using the CDD (Conserved Domain Database) tool in NCBI. The bootstrap values are indicated on the nodes based on 1000 trials. The asterisk indicates the characterized GLOxes.

2.2. Catalytic Properties of MtGLOx

The Amplex red assay was used to quantify H_2O_2 production to provide more sensitive measurement than the ABTS assay used in other studies [27,46]. Moreover, no addition of H_2O_2 was necessary to activate the purified MtGLOx (Figure S1) or eliminate the lag period, as described for other characterized glyoxal oxidases [26,27]. From our HPLC analysis and unlike other described glyoxal oxidases, the native enzyme from *M. thermophyla* is fully active even in the absence of auxiliary peroxidases or oxidizing agents. Activity screening of MtGLOx against common substrates for AA5_1 family members (Table 1) demonstrated higher activity of the enzyme against small aldehydes, such as methylglyoxal ($\sim 3.5 \text{ U mg}^{-1}$) than against glycerol. Moreover, HMF was found to be a previously unidentified substrate for GLOxes. The kinetic constants on the tested substrates are given in Table 2. MtGLOx oxidizes methylglyoxal and 5-HMF with almost the same catalytic efficiency and 10-fold higher when compared with glycerol as substrate. The oxidation product of the new substrate 5-HMF was 2,5-diformylfuran (DFF) and not 5-hydroxymethyl-2-furancarboxylic acid (HMFOA) (Figure 2). DFF is also a valuable compound with several applications for pharmaceuticals production [47], polymer resin synthesis [9], and material science [48]. Interestingly, this result shows that the oxidation pathway of 5-HMF leads to preferential conversion of the primary alcohol arm to an aldehyde instead of aldehyde to carboxylic acid (Figure 2A,B). The time course reaction shows that MtGLOx oxidized 56% of the HMF in 24 h (Figure 2C) but it was unable to further oxidize DFF. Low conversion levels were also observed for other characterized GLOxes [25,27] and for a new AA5_2 from *Colletotrichum gramimicola* able to oxidize 1-butanol to butanal [33]. A possible autooxidation of 5-HMF in solution was discarded, as can be seen in the reaction control (Figure S2A). The low yields have been attributed to oxidative

damage that is caused by H_2O_2 , acidification, in the case of carboxylic acid products, or end-product inhibition [25]. In the case of *MtGLOx*, the hypothesis of H_2O_2 oxidative damage was not supported by our experimental results, since catalase addition was unable to promote an increased *MtGLOx* activity (Figure S2B). The same phenomenon was observed for *GLOx* from *P. chrysosporium* [25].

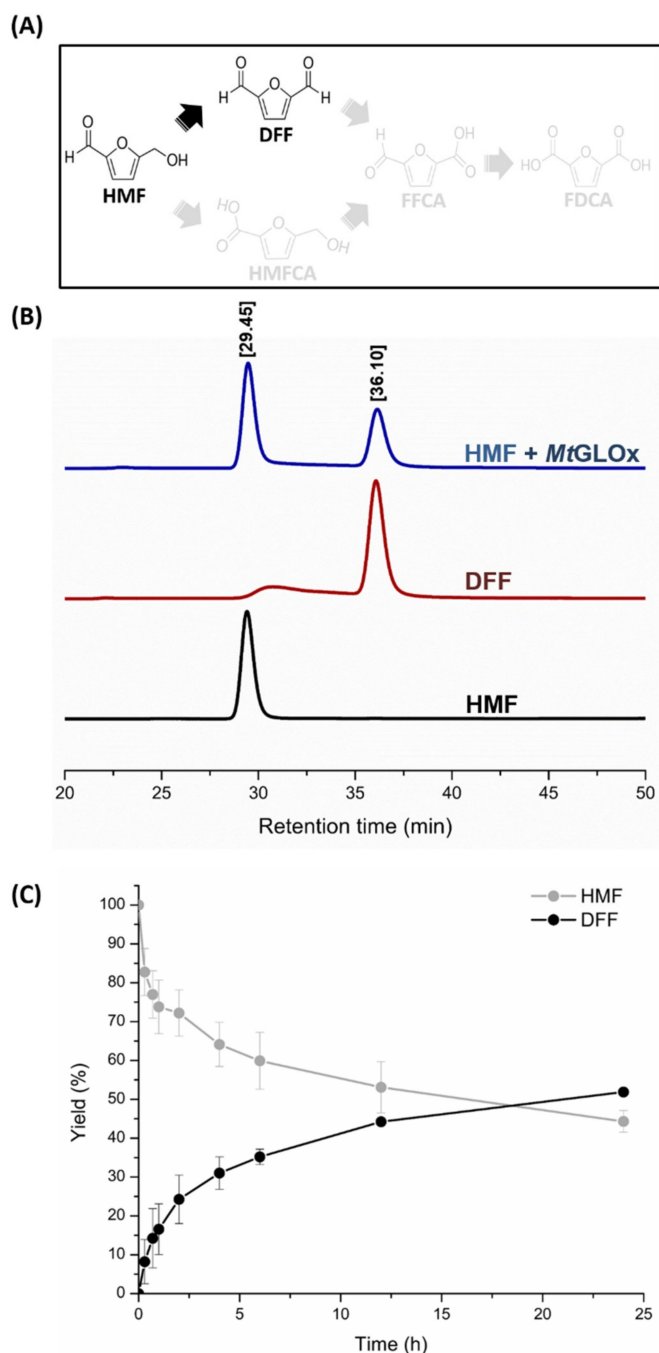


Figure 2. Pathway followed by *MtGLOx* for hydroxymethylfurfural (HMF) oxidation. (A) Representation of possible pathways of hydroxymethylfurfural (HMF) oxidation and products. *MtGLOx* oxidizes HMF only to 2,5-dimethylfuran (DFF) (black path). (B) High Performance Liquid Chromatography (HPLC) chromatograms of the products generated from HMF oxidation. Blue line: product generated from HMF oxidation. Red and black lines: DFF and HMF standards, respectively. Reaction mixture were incubated for 24 h (blue). (C) Time course reactions were monitored for oxidation of 1 mM HMF to DFF by 0.5 μ M *MtGLOx*. Standard deviations are shown by error bars ($n = 3$).

Table 1. Substrate specificity of *MtGLOx*.

Substrate	$\mu\text{mol H}_2\text{O}_2 \cdot \text{min}^{-1} \cdot \text{mg}^{-1} \text{enz}$	Relative Activity (%)
5-HMF	3.58 ± 0.07	100
Methylglyoxal	3.45 ± 0.11	96
Glycerol	0.57 ± 0.06	16
Formaldehyde	0.16 ± 0.01	4
Furfural	ND	ND
DFF	ND	ND
Glutaraldehyde	ND	ND

The specificity test was done with 25 mM of each substrate and 0.5 μM enzyme at 50 °C for 5 min. The values are the mean of three replicates. ND: not detected activity.

Table 2. Kinetic parameters of *MtGLOx* with different substrates.

Substrate	V_{max} (nkat·mg ⁻¹)	K_{M} (mM)	k_{cat} (s ⁻¹)	$k_{\text{cat}}/K_{\text{M}}$ (mM ⁻¹ ·s ⁻¹)
Methylglyoxal	123.3 ± 17.0	12.8 ± 2.6	12.6	0.99
5-HMF	156.1 ± 15.8	20.2 ± 9.0	15.9	0.86
Glycerol	333.7 ± 16.4	471.3 ± 88.7	34.1	0.07

A selective oxidation mechanism of primary alcohols to aldehydes has been previously described for a flavoenzyme, aryl-alcohol oxidase [49]. The preferential oxidation of HMF to DFF has also been shown for galactose oxidases [49], and in combination with aldehyde oxidases, can lead to FDCA (2,5-furandicarboxylic acid), a bioplastic precursor, production [10] (Figure 2A).

The maximum activity of *MtGLOx* was observed at pH 6.0 and 50 °C (Figure 3A,B). These optimum conditions for *MtGLOx* were practically the same as described for the two glyoxal oxidases from *P. cinnabarinus* [27], but distinct from the *P. chrysosporium* enzyme (30 °C and pH 5.0) [38]. The residual activity after incubation at various temperatures was assayed at pH 6.0 using methylglyoxal as a substrate. *MtGLOx* maintained its activity at 50 °C and 60 °C for 4 h, but lost 50% of its initial activity after 15 min at 70 °C (Figure 3B). *MtGLOx* reveals higher thermostability than *P. cinnabarinus* glyoxal oxidases.

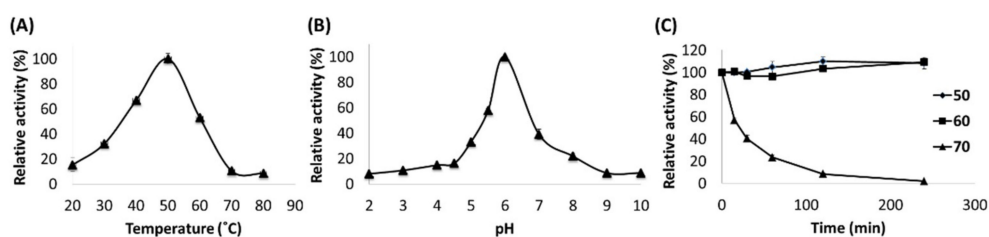


Figure 3. Effect of pH and temperature on enzymatic activity. Effect of temperature (A) and pH (B) on enzymatic activity of *MtGLOx*. Values calculated as a percentage of the activity at the maximum. (C) The enzyme residual activity after incubation at different temperature is represented as a percentage with respect to the enzyme initial activity at different incubation times.

2.3. Catalytic Domain and Copper Site of *MtGLOx*

The three-dimensional structure of the *MtGLOx* catalytic domain was homology modeled using the crystal structure of the cuproenzyme GlxA from *Streptomyces lividans* (PDBid: 4UNM) [39] as a template. The model suggested a similar fold to that of galactose and alcohol oxidases from family AA5 that is composed mostly of β -sheets [33,50]. The model highlights an N-terminal β -propeller structure containing the catalytic copper center linked to a C-terminal immunoglobulin-like domain, with both domains being involved in forming the active site of *MtGLOx* (Figure 4A). The copper region is exposed to the solvent environment. Based on sequence alignment, and the three-dimensional structure model, residues His804, His889, and Tyr803 that compose the first-shell coordination of the

copper ion and Cys522-Tyr581 that stabilize the free-radical species [50] are all conserved between glyoxal, galactose, alcohol oxidases, and GlxA copper-radical oxidase from the AA5 family (Figure 4B). In the second-shell coordination, a tryptophan residue that lies over the Tyr581-Cys522 is associated with substrate recognition, catalysis, and radical stabilization [51–53]. In AA5_1 members, the Trp580 residue is conserved and is adjacent to Tyr581 unlike AA5_2 members (Figure 4B). The galactose oxidase structure from *F. graminearum* [50] shows this residue conserved in the same position but 17 residues away from Tyr. On the other hand, the alcohol oxidase from *C. graminicola* [33] shows the Tyr residue replaced by Phe138.

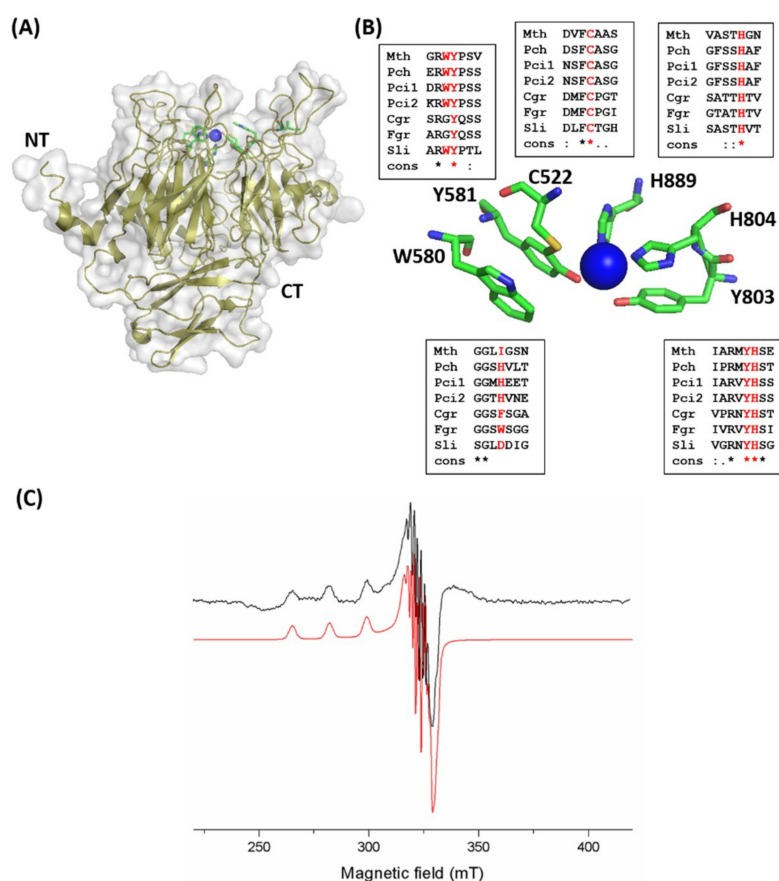


Figure 4. Structural model and spectroscopy of the *MtGLOx* Cu center. **(A)** Cartoon representation of the model of the catalytic domain of *MtGLOx*. **(B)** Stick model of the substrate pocket showing the conserved residues coordinating the copper ion (blue sphere). Sections of the sequence from the characterized glyoxal oxidases from *P. chrysosporium* (Pch) and *Pycnoporus cinnabarinus* (Pci1 and 2), alcohol oxidase from *Colletotrichum graminicola* (Cgr), galactose oxidase from *Fusarium graminearum* (Fgr) and cuproenzyme from *Streptomyces lividans* (Sli) showing conserved amino acids. **(C)** Cu(II)-*MtGLOx* EPR spectrum (black) with simulation (red).

The EPR spectrum of *MtGLOx* (Figure 4C) is characteristic of a mononuclear Cu(II) center with an axial coordination, which is in good agreement with previous EPR data from related enzymes [33]. Although the Cu(I) state cannot be directly detected by EPR, our experimental EPR spectra clearly demonstrate a strong signal from a Cu(II) ion that is bound to the active site of the enzyme. The superhyperfine lines that were observed in the perpendicular direction of the spectrum indicate the interaction of the copper ion with other nuclei in its vicinity. To further characterize the paramagnetic center, we performed spectral simulation using the Easy Spin package. A spin Hamiltonian containing terms that took into account the Zeeman, hyperfine, and superhyperfine interactions was used. A good agreement with the experimental spectrum was obtained by including two nitrogen nuclei and the following magnetic parameters: $g_x = g_y = 2.05$ and $g_z = 2.28$; $|A_x| = |A_y| = 60$ MHz

and $|A_z| = 540$ MHz. The superhyperfine couplings to the nitrogen nuclei were 40 MHz. These parameters indicate a main $d(x^2-y^2)$ character for the copper molecular orbital, as observed for other copper-radical oxidases [32,33], and suggest that the *MtGLOx* active site contains the main structural features that are characteristic for the AA5_1 enzyme family.

2.4. Structural Insights of the Multi-Domain *MtGLOx* by SAXS

SAXS were used to infer a low-resolution envelope of the enzyme, determine the relative arrangements of the four WSC domains to the catalytic domain in solution. This method was used following unsuccessful crystallization attempts. The SAXS curve profile and linear radius of gyration (R_g) of 45.3 Å indicates an aggregation-free state and a maximal dimension (D_{max}) of 155 Å suggesting an elongated shape (Figure 5A,B). The pair distribution function ($P(r)$) also shows a maximum at ~30 Å from pair electron distances within the catalytic domain (CD) and a secondary shoulder at ~90 Å that is attributed to distances between the CD and the WSC domains (Figure 5B). The molecular weight that was predicted by SAXS_MoW for *MtGLOx* was 99 kDa, in agreement with the theoretical 102 kDa of the monomer. Ab initio molecular envelope reconstruction of *MtGLOx* allowed modeling two regions that could accommodate the WSC domains and the catalytic domain (Figure 5D). To better address this issue, the structure of each domain was modeled based on its amino acid sequence, linked by polyalanine linkers, and allowed to move as rigid bodies using molecular dynamic simulations. The best model generated shows an excellent fit ($\chi = 1.7$) with the experimental curve and fits closely to the low-resolution SAXS molecular envelope, discarding significant large-amplitude inter-domain dynamic or conformational changes. The WSC1-WSC2 and WSC4-WSC3-AA5_1 three-dimensional structural models are connected by a longer and flexible linker, as supported by the Kratky plot (Figure 5C), but not perfectly aligned and appear instead in a bent conformation. The SAXS data also show that the WSC domains are probably connected to the catalytic domain by their upper region (Figure 5B), where the buried copper co-factor resides. Moreover, the low-resolution model allows us to propose that the WSC domains could act as an anchor that orient the catalytic site at the substrate's surface.

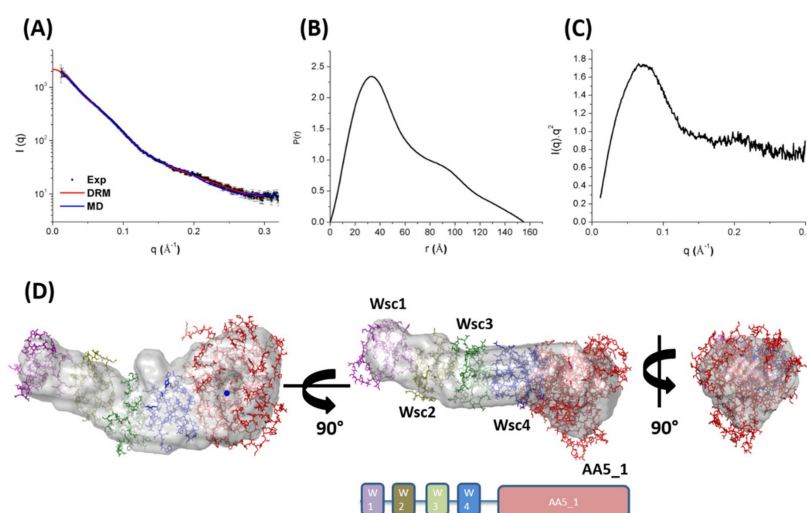


Figure 5. Solution structure of *MtGLOx*. (A) Small Angle X-ray Scattering (SAXS) data. Raw data: plot of scattered intensity vs. scattering angle q . Experimental SAXS curve is shown in black filled circles. The fit of the molecular envelope (red line) and molecular dynamic model (blue line). Exp: experimental raw data. DRM: dammy residue modelling fit. MD: molecular dynamic model fit. (B) Pair distribution function $P(r)$. (C) Kratky plot. (D) Ab initio envelope models based on SAXS data. Molecular envelope superimposed on the three-dimensional model of each domain. The Ab initio envelope is represented in gray. Each domain is represented in stick form. The blue sphere highlights the position of the copper co-factor center.

3. Material and Methods

3.1. Chemicals and Reagents

Chemicals, biochemicals and enzymes were obtained from Fisher Scientific (Pittsburgh, PA, USA), Invitrogen, Merck (Darmstadt, Germany) or Sigma-Aldrich (St. Louis, MO, USA).

3.2. Expression and Purification

The *MtGLOx* gene (MYCTH_2294895) from *Myceliophthora thermophila* M77 was PCR amplified from genomic DNA without the original signal peptide. The PCR product was amplified using the oligonucleotide primers forward (5'-GGGTTGGCACAGCTCTCAATCCCTACGGACCTTCCGGA-3') and reverse (5-GTCCCGTGCCGGTTATCAGACGCCGGGACAGAAAAGTCGGGGCGC-3) and was cloned into the pEXPYR vector [54] using the Ligation-Independent Cloning protocol (LIC) [55]. The clone was transformed in *A. nidulans* A773, as described [54].

Approximately 10^7 spores/mL were inoculated in liquid minimal medium supplemented with 5% maltose and maintained in static culture at 37 °C for 40 h. The culture medium was filtered using Miracloth membrane (Calbiochem, San Diego, CA, USA). The secreted proteins were concentrated by tangential flow filtration (GE Healthcare, Uppsala, Sweden) and were immediately applied to a DEAE-Sephadex column (GE Healthcare). The enzyme was eluted with a stepwise gradient (200, 300, 400, and 500 mM) NaCl in 50 mM Tris-HCl pH 8.0. The purified samples were concentrated by ultrafiltration (50 kDa cutoff Centricon-Millipore, Billerica, MA, USA) and further purified using size exclusion chromatography on a HiLoad 16/60 Sephadex75 column (GE Healthcare) with a running buffer consisting of 150 mM NaCl and 20 mM Tris-HCl pH 8.0. The total protein was quantified spectrophotometrically at 280 nm using a molar extinction coefficient of 168550. The protein purity was analyzed by SDS-PAGE [56], stained with Coomassie blue G-250, and the protein identity was confirmed by mass spectrometry.

3.3. Mass Spectrometry

The peptide mass fingerprint was performed by in-gel digestion. The Coomassie stained protein band was removed from the SDS-PAGE 15% gel and was submitted to in-gel trypsin (20 ng/ μ L) digestion after its reduction and alkylation. An aliquot of digested product (1 μ L) was desalted by a ZipTip C18 column and mixed with 1 μ L of alpha-cyano-4-hydroxy cinnamic acid (HCCA) matrix at 10 mg/mL and was allowed to dry over the sample plate. The measurement was done in the linear positive-ion mode at room temperature within a range of 400–3300 m/z . Average masses were assigned and processed using flexAnalysisTM software (Bruker Daltonics, Bremen, Germany). The mass fingerprint search was done using BioToolsTM (Bruker Daltonics) and the peptide m/z list generated in silico by computational tryptic digestion of protein amino acid sequence. The peptide fingerprinting match was also performed using the MASCOT (Matrix Science Inc.). The analysis was performed using a Microflex LT MALDI-TOF (Bruker Daltonics).

3.4. Enzyme Activity Assay and Steady-State Kinetics

MtGLOx activity was determined measuring hydrogen peroxide (H_2O_2) production using a subsequent reaction with horseradish peroxidase (HRP) and Amplex[®] Red reagent (Thermo Fisher Scientific, Bremen Germany). The enzyme-coupled reaction protocol was modified due to the differences in optimum reaction conditions between *MtGLOx* and HRP. The reaction mixture (100 μ L) containing 0.5 μ M *MtGLOx*, 10 mM Bis-Tris (pH 6.0), and 25 mM substrate was incubated for 5 min at optimum temperature. The second reaction was started by addition of 10 μ L of the previous reaction to 90 μ L of Amplex Red working solution according to the manufacturer. The H_2O_2 production was measured using oxidized Amplex Red absorbance at 560 nm on a Tecan Infinite M200 microtiter plate reader. All of the measurements were performed in triplicate. The optimum pH and temperature were determined using 25 mM methylglyoxal as substrate in citrate-glycine-phosphate buffer. The

temperature stability of the enzyme was measured by determining residual activity after incubating the enzyme at 50, 60, and 70 °C, followed by cooling in ice and activity measurement.

The kinetic constants were determined at optimum temperature and pH using the protocol described above. The kinetic parameters were determined using a substrate range of 1–40 mM for methylglyoxal/5-HMF and 10–500 mM for glycerol. Data analysis was performed using a non-linear regression of the Michaelis-Menten equation on GraphPad Prism v5.1 software (GraphPad Software, La Jolla, CA, USA).

3.5. Analysis of Oxidized Products

The oxidized products of *MtGLOx* catalytic activity were analyzed by High Performance Liquid Chromatography (HPLC), using a Bio-Rad Aminex HPX-87H column (300 mm × 7.8 mm) (Bio-Rad, Hercules, CA, USA). Chromatography was carried out at 65 °C with 5 mM sulfuric acid as mobile phase at a flow rate of 0.6 mL/min. Eluted peaks of 5-HMF and DFF were detected by UV absorption at 276 nm. The time course of oxidation of HMF (1 mM) by *MtGLOx* (0.5 μM) was performed in 100 mM Bis-Tris pH 6.0. The same reaction was monitored using 670 U/mL of catalase from *Aspergillus niger* (Sigma-Aldrich). Aliquots (60 μL) of the reaction were diluted with 300 μL water and 60 μL 1 M HCl. The solution containing denatured protein was centrifuged and the supernatant was used for injection onto the column. Purified HMF and DFF (Sigma-Aldrich) were used as standards.

3.6. Small Angle X-ray Scattering (SAXS) Experiments

MtGLOx was prepared at concentrations of 1, 2, and 4 mg/mL in 50 mM Tris-HCl (pH 8.0) and 150 mM NaCl. SAXS data were collected through mail-in-SAXS on the 12.3.1 SIBYLS beamline at the Advanced Light Source, Lawrence Berkeley National Laboratory [57]. Scattering from the buffer was subtracted from sample scattering and was checked for agreement. The raw data were processed using PRIMUS [58] and GNOM [59]. Twenty low-resolution envelope models were generated using GASBOR [60] and were averaged with DAMAVER [61]. The three-dimensional model of each *MtGLOx* domain was generated using the iTasser server [62] and available structures of the cuproenzyme GalxA from *Streptomyces lividans* (PDBid: 4UNM) [39] and WSC domain from the human Wnt modulator (PDBid: 5FWW) [63] as templates. The relative position of each domain based on SAXS data was determined using a combination of conformational sampling and molecular dynamics performed on the BILBOMD server [64]. The final model and low resolution envelope superposition was performed using SUPERCOMB [65]. The molecular weight based on the SAXS data was calculated using SAXS MoW [66].

3.7. Electron Paramagnetic Resonance (EPR) Spectroscopy

EPR experiments were performed on a Varian E109 spectrometer equipped with a cryogenic system, which allowed for low-temperature data collection. The spectrometer was operated at 9.26 GHz, with a modulation amplitude of 4 G and microwave power of 10 mW, at 70 K. Samples were drawn into quartz tubes and were then frozen in liquid nitrogen. The EPR parameters were optimized to avoid line saturation and distortion. The spectrum of the buffer only was used as a baseline and was subtracted from all other spectra. Spectral simulations of the EPR data were performed using the EasySpin package [67]. The spin Hamiltonian included terms to account for the Zeeman and hyperfine interactions, which yielded the calculated *g*- and *A*-values.

3.8. Sequence and Domain Analysis

The AA5_1 domain sequence of 47 glyoxal oxidases from 39 different organisms were aligned using MUSCLE software [68]. For comparison purposes, an identity tree was generated using the Neighbor-joining (NJ) method that was implemented using the MEGA software [69]. The domain composition of each GLOX was annotated using the CDD (Conserved Domain Database) tool in NCBI.

4. Conclusions

The core cellulase secretome of *M. thermophila* comprises the classical set of hydrolytic cellobiohydrolases (GH6/GH7), beta-glucosidase (GH3), and the oxidative enzymes cellobiose dehydrogenase (AA3), lytic polysaccharide monooxygenases (AA9), aryl-alcohol oxidase (AA3), glyoxal oxidase (AA5_1), and an unknown GMC oxidoreductase. Oxizymes are able to produce hydrogen peroxide and have been suggested to be coupled to ligninolytic peroxidases. However, fungi such as *M. thermophila* do not secrete this class of peroxidases. Suggesting another unknown role for MtGLOx. Here, we characterize a new multi-domain glyoxal oxidase that produces hydrogen peroxide as a second reaction and oxidizes the fermentation inhibitor HMF. This activity suggests possible green applications of MtGLOx as an enzyme for raw biomass byproduct conversion into sustainable chemical product. Moreover, MtGLOx is the first glyoxal oxidase reported to be connected to four unknown domains, called WSC. However, based on sequence analysis, a substantial number of fungal multidomain AA5_1 members are linked to WSC domains at the N-terminus. This is the same location where either a transmembrane helix [39] or a globular domain 1 related to binding to extracellular carbohydrate [70] can be found in the closely related galactose oxidases. A WSC domain is considered to be a functionally variable putative carbohydrate binding domain [40] able to mediate sensor clustering in stress conditions [42]. However, the specific target of such a domain remains to be elucidated. The overall architecture and spatial arrangement of this multi-domain enzyme was revealed by SAXS data and it describes MtGLOx as a monomeric enzyme in an extended conformation in solution.

Supplementary Materials: The following are available online at <http://www.mdpi.com/2073-4344/8/10/476/s1>, Figure S1. Identification of the purified MtGLOx heterologously expressed and secreted by *Aspergillus nidulans*. (A) SDS-PAGE showing the purified MtGLOx. MW: molecular weight. (B) MALDI-TOF/MS peptide mass fingerprint analysis of MtGLOx. Mass spectrum profile in the m/z range 800–3300 Da. The peptide mass fingerprint was made from fragments of MtGLOx after tryptic digestion. Green dots mark the expected tryptic masses that matches the theoretical m/z with a maximum 2 Da tolerance. (C) Protein identification and sequence coverage after m/z list analysis. The sequence coverage of the tryptic fragments is shown in bold red (31% coverage). Figure S2. Reaction controls of the time course oxidation of HMF by MtGLOx. (A) Effect of HMF incubation in 100 mM Bis-Tris pH 6.0. (B) Effect of catalase on time course conversion of HMF to DFF. The time course oxidation of HMF (1 mM) by MtGLOx (0.5 μ M) in 100 mM Bis-Tris pH 6.0. The reaction was monitored by DFF quantification by High Performance Liquid Chromatography (HPLC), using a Bio-Rad Aminex HPX-87H column with and without 670 U/mL of catalase from *Aspergillus niger* (Sigma-Aldrich).

Author Contributions: M.A.S.K., I.P. and R.A.P. designed the experiments; M.A.S.K. and M.O.d.G. performed the gene cloning, expression and purification; M.A.S.K. and M.O.d.G. characterized the enzymatic activities; M.A.S.K. performed HPLC analysis; M.A.S.K. treated SAXS data; J.A.C.F. and P.S.K. performed EPR experiments and data analysis; M.A.S.K., I.P. and R.A.P. wrote the manuscript with the input from all the other authors; A.M., I.P. and R.A.P. supervised the project.

Funding: This research was financially supported by Fundação de Amparo à Pesquisa do Estado de São Paulo (FAPESP) via grants 2011/20505-4 and 2015/13684-0 and by Conselho Nacional de Desenvolvimento Científico e Tecnológico (CNPq) via grants 405191/2015-4, 303988/2016-9, 440977/2016-9 and 151963/2018-5 and by Coordenação de Aperfeiçoamento de Pessoal de Nível Superior (CAPES).

Conflicts of Interest: The authors declare no conflicts of interest.

References

1. Sanchez, C. Lignocellulosic residues: Biodegradation and bioconversion by fungi. *Biotechnol. Adv.* **2009**, *27*, 185–194. [[CrossRef](#)] [[PubMed](#)]
2. Scheller, H.V.; Ulvskov, P. Hemicelluloses. *Annu. Rev. Plant Biol.* **2010**, *61*, 263–289. [[CrossRef](#)] [[PubMed](#)]
3. Higuchi, T. Lignin biochemistry: Biosynthesis and biodegradation. *Wood Sci. Technol.* **1990**, *24*, 3–63. [[CrossRef](#)]
4. Jonsson, L.J.; Alriksson, B.; Nilvebrant, N.O. Bioconversion of lignocellulose: Inhibitors and detoxification. *Biotechnol. Biofuels* **2013**, *6*, 16. [[CrossRef](#)] [[PubMed](#)]
5. Mohanram, S.; Amat, D.; Choudhary, J.; Arora, A.; Nain, L. Novel perspectives for evolving enzyme cocktails for lignocellulose hydrolysis in biorefineries. *Sustain. Chem. Process.* **2013**, *1*, 15. [[CrossRef](#)]

6. Klinke, H.B.; Thomsen, A.B.; Ahring, B.K. Inhibition of ethanol-producing yeast and bacteria by degradation products produced during pre-treatment of biomass. *Appl. Microbiol. Biotechnol.* **2004**, *66*, 10–26. [[CrossRef](#)] [[PubMed](#)]
7. Agblevor, F.A.; Jahromi, H. Aqueous-Phase Synthesis of Hydrocarbons from Furfural Reactions with Low-Molecular-Weight Biomass Oxygenates. *Energy Fuels* **2018**, *32*, 8552–8562. [[CrossRef](#)]
8. Rosatella, A.A.; Simeonov, S.P.; Frade, R.F.M.; Afonso, C.A.M. 5-Hydroxymethylfurfural (HMF) as a building block platform: Biological properties, synthesis and synthetic applications. *Green Chem.* **2011**, *13*, 754–793. [[CrossRef](#)]
9. Amarasekara, A.S.; Green, D.; Williams, L.D. Renewable resources based polymers: Synthesis and characterization of 2,5-diformylfuran–urea resin. *Eur. Polym. J.* **2009**, *45*, 595–598. [[CrossRef](#)]
10. McKenna, S.M.L.S.; Herter, S.; Turner, N.J.; Carnell, A.J. Enzyme cascade reactions: Synthesis of furandicarboxylic acid (FDCA) and carboxylic acids using oxidases in tandem. *Green Chem.* **2015**, *17*, 3271–3275. [[CrossRef](#)]
11. Jahromi, H.; Agblevor, F.A. Hydrodeoxygenation of Aqueous-Phase Catalytic Pyrolysis Oil to Liquid Hydrocarbons Using Multifunctional Nickel Catalyst. *Ind. Eng. Chem. Res.* **2018**, *57*, 13257–13268. [[CrossRef](#)]
12. Berka, R.M.; Grigoriev, I.V.; O'tillar, R.; Salamov, A.; Grimwood, J.; Reid, I.; Ishmael, N.; John, T.; Darmond, C.; Moisan, M.C.; et al. Comparative genomic analysis of the thermophilic biomass-degrading fungi *Myceliophthora thermophila* and *Thielavia terrestris*. *Nat. Biotechnol.* **2011**, *29*, 922–927. [[CrossRef](#)] [[PubMed](#)]
13. Dos Santos, H.B.; Bezerra, T.M.; Pradella, J.G.; Delabona, P.; Lima, D.; Gomes, E.; Hartson, S.D.; Rogers, J.; Couger, B.; Prade, R. *Myceliophthora thermophila* M77 utilizes hydrolytic and oxidative mechanisms to deconstruct biomass. *AMB Express* **2016**, *6*, 1–12. [[CrossRef](#)] [[PubMed](#)]
14. Divne, C.; Stahlberg, J.; Reinikainen, T.; Ruohonen, L.; Pettersson, G.; Knowles, J.K.; Teeri, T.T.; Jones, T.A. The three-dimensional crystal structure of the catalytic core of cellobiohydrolase I from *Trichoderma reesei*. *Science* **1994**, *265*, 524–528. [[CrossRef](#)] [[PubMed](#)]
15. Eriksson, K.E.; Pettersson, B.; Westermark, U. Oxidation: An important enzyme reaction in fungal degradation of cellulose. *FEBS Lett.* **1974**, *49*, 282–285. [[CrossRef](#)]
16. Villares, A.; Moreau, C.; Bennati-Granier, C.; Garajova, S.; Foucat, L.; Falourd, X.; Saake, B.; Berrin, J.G.; Cathala, B. Lytic polysaccharide monoxygenases disrupt the cellulose fibers structure. *Sci. Rep.* **2017**, *7*, 1–9. [[CrossRef](#)] [[PubMed](#)]
17. Vaaje-Kolstad, G.; Westereng, B.; Horn, S.J.; Liu, Z.L.; Zhai, H.; Sorlie, M.; Eijsink, V.G.H. An Oxidative Enzyme Boosting the Enzymatic Conversion of Recalcitrant Polysaccharides. *Science* **2010**, *330*, 219–222. [[CrossRef](#)] [[PubMed](#)]
18. Eastwood, D.C.; Floudas, D.; Binder, M.; Majcherczyk, A.; Schneider, P.; Aerts, A.; Asiegbu, F.O.; Baker, S.E.; Barry, K.; Bendiksby, M.; et al. The plant cell wall-decomposing machinery underlies the functional diversity of forest fungi. *Science* **2011**, *333*, 762–765. [[CrossRef](#)] [[PubMed](#)]
19. Gudrun, G.; Willem, J.H.V.B. Oxizymes for Biotechnology. *Curr. Biotechnol.* **2015**, *4*, 100–110. [[CrossRef](#)]
20. Whittaker, M.M.; Kersten, P.J.; Cullen, D.; Whittaker, J.W. Identification of catalytic residues in glyoxal oxidase by targeted mutagenesis. *J. Biol. Chem.* **1999**, *274*, 36226–36232. [[CrossRef](#)] [[PubMed](#)]
21. Daou, M.; Faulds, C.B. Glyoxal oxidases: Their nature and properties. *World J. Microbiol. Biotechnol.* **2017**, *33*, 87. [[CrossRef](#)] [[PubMed](#)]
22. Cantarel, B.L.; Coutinho, P.M.; Rancurel, C.; Bernard, T.; Lombard, V.; Henrissat, B. The Carbohydrate-Active EnZymes database (CAZy): An expert resource for Glycogenomics. *Nucleic Acids Res.* **2009**, *37*, D233–D238. [[CrossRef](#)] [[PubMed](#)]
23. Levasseur, A.; Drula, E.; Lombard, V.; Coutinho, P.M.; Henrissat, B. Expansion of the enzymatic repertoire of the CAZy database to integrate auxiliary redox enzymes. *Biotechnol. Biofuels* **2013**, *6*, 41. [[CrossRef](#)] [[PubMed](#)]
24. Whittaker, J.W. The radical chemistry of galactose oxidase. *Arch. Biochem. Biophys.* **2005**, *433*, 227–239. [[CrossRef](#)] [[PubMed](#)]
25. Roncal, T.; Munoz, C.; Lorenzo, L.; Maestro, B.; Diaz de Guereny Mdel, M. Two-step oxidation of glycerol to glyceric acid catalyzed by the *Phanerochaete chrysosporium* glyoxal oxidase. *Enzym. Microb. Technol.* **2012**, *50*, 143–150. [[CrossRef](#)] [[PubMed](#)]

26. Kersten, P.J. Glyoxal oxidase of *Phanerochaete chrysosporium*: Its characterization and activation by lignin peroxidase. *Proc. Natl. Acad. Sci. USA* **1990**, *87*, 2936–2940. [[CrossRef](#)] [[PubMed](#)]
27. Daou, M.; Piumi, F.; Cullen, D.; Record, E.; Faulds, C.B. Heterologous production and characterization of two glyoxal oxidases from *Pycnoporus cinnabarinus*. *Appl. Environ. Microbiol.* **2016**. [[CrossRef](#)] [[PubMed](#)]
28. Thornalley, P.J.; Langborg, A.; Minhas, H.S. Formation of glyoxal, methylglyoxal and 3-deoxyglucosone in the glycation of proteins by glucose. *Biochem. J.* **1999**, *344 Pt 1*, 109–116. [[CrossRef](#)]
29. Kersten, P.J.; Kirk, T.K. Involvement of a new enzyme, glyoxal oxidase, in extracellular H₂O₂ production by *Phanerochaete chrysosporium*. *J. Bacteriol.* **1987**, *169*, 2195–2201. [[CrossRef](#)] [[PubMed](#)]
30. Yamada, Y.; Wang, J.; Kawagishi, H.; Hirai, H. Improvement of ligninolytic properties by recombinant expression of glyoxal oxidase gene in hyper lignin-degrading fungus *Phanerochaete sordida* YK-624. *Biosci. Biotechnol. Biochem.* **2014**, *78*, 2128–2133. [[CrossRef](#)] [[PubMed](#)]
31. Kersten, P.; Cullen, D. Copper radical oxidases and related extracellular oxidoreductases of wood-decay Agaricomycetes. *Fungal Genet. Biol. FG B* **2014**, *72*, 124–130. [[CrossRef](#)] [[PubMed](#)]
32. Whittaker, M.M.; Kersten, P.J.; Nakamura, N.; Sanders-Loehr, J.; Schweizer, E.S.; Whittaker, J.W. Glyoxal oxidase from *Phanerochaete chrysosporium* is a new radical-copper oxidase. *J. Biol. Chem.* **1996**, *271*, 681–687. [[CrossRef](#)] [[PubMed](#)]
33. Yin, D.T.; Urresti, S.; Lafond, M.; Johnston, E.M.; Derikvand, F.; Ciano, L.; Berrin, J.G.; Henrissat, B.; Walton, P.H.; Davies, G.J.; et al. Structure-function characterization reveals new catalytic diversity in the galactose oxidase and glyoxal oxidase family. *Nat. Commun.* **2015**, *6*, 10197. [[CrossRef](#)] [[PubMed](#)]
34. Leuthner, B.; Aichinger, C.; Oehmen, E.; Koopmann, E.; Muller, O.; Muller, P.; Kahmann, R.; Bolker, M.; Schreier, P.H. A H₂O₂-producing glyoxal oxidase is required for filamentous growth and pathogenicity in *Ustilago maydis*. *Mol. Genet. Genom. MGG* **2005**, *272*, 639–650. [[CrossRef](#)] [[PubMed](#)]
35. Song, X.S.; Xing, S.; Li, H.P.; Zhang, J.B.; Qu, B.; Jiang, J.H.; Fan, C.; Yang, P.; Liu, J.L.; Hu, Z.Q.; et al. An antibody that confers plant disease resistance targets a membrane-bound glyoxal oxidase in *Fusarium*. *New Phytol.* **2016**, *210*, 997–1010. [[CrossRef](#)] [[PubMed](#)]
36. Verna, J.; Lodder, A.; Lee, K.; Vagts, A.; Ballester, R. A family of genes required for maintenance of cell wall integrity and for the stress response in *Saccharomyces cerevisiae*. *Proc. Natl. Acad. Sci. USA* **1997**, *94*, 13804–13809. [[CrossRef](#)] [[PubMed](#)]
37. Futagami, T.; Nakao, S.; Kido, Y.; Oka, T.; Kajiwara, Y.; Takashita, H.; Omori, T.; Furukawa, K.; Goto, M. Putative stress sensors WscA and WscB are involved in hypo-osmotic and acidic pH stress tolerance in *Aspergillus nidulans*. *Eukaryot. Cell* **2011**, *10*, 1504–1515. [[CrossRef](#)] [[PubMed](#)]
38. Son, Y.L.; Kim, H.Y.; Thiyagarajan, S.; Xu, J.J.; Park, S.M. Heterologous Expression of *Phanerochaete chrysosporium* Glyoxal Oxidase and its Application for the Coupled Reaction with Manganese Peroxidase to Decolorize Malachite Green. *Mycobiology* **2012**, *40*, 258–262. [[CrossRef](#)] [[PubMed](#)]
39. Chaplin, A.K.; Petrus, M.L.; Mangiameli, G.; Hough, M.A.; Svistunen, D.A.; Nicholls, P.; Claessen, D.; Vijgenboom, E.; Worrall, J.A. GlxA is a new structural member of the radical copper oxidase family and is required for glycan deposition at hyphal tips and morphogenesis of *Streptomyces lividans*. *Biochem. J.* **2015**, *469*, 433–444. [[CrossRef](#)] [[PubMed](#)]
40. Tong, S.M.; Chen, Y.; Zhu, J.; Ying, S.H.; Feng, M.G. Subcellular localization of five singular WSC domain-containing proteins and their roles in *Beauveria bassiana* responses to stress cues and metal ions. *Environ. Microbiol. Rep.* **2016**, *8*, 295–304. [[CrossRef](#)] [[PubMed](#)]
41. Cohen-Kupiec, R.; Broglie, K.E.; Friesem, D.; Broglie, R.M.; Chet, I. Molecular characterization of a novel beta-1,3-exoglucanase related to mycoparasitism of *Trichoderma harzianum*. *Gene* **1999**, *226*, 147–154. [[CrossRef](#)]
42. Heinisch, J.J.; Dupres, V.; Wilk, S.; Jendretzki, A.; Dufrene, Y.F. Single-molecule atomic force microscopy reveals clustering of the yeast plasma-membrane sensor Wsc1. *PLoS ONE* **2010**, *5*, e11104. [[CrossRef](#)] [[PubMed](#)]
43. Floudas, D.; Binder, M.; Riley, R.; Barry, K.; Blanchette, R.A.; Henrissat, B.; Martinez, A.T.; Otilar, R.; Spatafora, J.W.; Yadav, J.S.; et al. The Paleozoic origin of enzymatic lignin decomposition reconstructed from 31 fungal genomes. *Science* **2012**, *336*, 1715–1719. [[CrossRef](#)] [[PubMed](#)]
44. Bissaro, B.; Rohr, A.K.; Muller, G.; Chylenski, P.; Skaugen, M.; Forsberg, Z.; Horn, S.J.; Vaaje-Kolstad, G.; Eijsink, V.G.H. Oxidative cleavage of polysaccharides by monocopper enzymes depends on H₂O₂. *Nat. Chem. Biol.* **2017**, *13*, 1123–1128. [[CrossRef](#)] [[PubMed](#)]

45. Lamb, C.; Dixon, R.A. The Oxidative Burst in Plant Disease Resistance. *Annu. Rev. Plant Physiol. Plant Mol. Biol.* **1997**, *48*, 251–275. [[CrossRef](#)] [[PubMed](#)]
46. Holland, J.T.; Harper, J.C.; Dolan, P.L.; Manginell, M.M.; Arango, D.C.; Rawlings, J.A.; Apblett, C.A.; Brozik, S.M. Rational redesign of glucose oxidase for improved catalytic function and stability. *PLoS ONE* **2012**, *7*, e37924. [[CrossRef](#)] [[PubMed](#)]
47. Hopkins, K.T.; Wilson, W.D.; Bender, B.C.; McCurdy, D.R.; Hall, J.E.; Tidwell, R.R.; Kumar, A.; Bajic, M.; Boykin, D.W. Extended aromatic furan amidino derivatives as anti-*Pneumocystis carinii* agents. *J. Med. Chem.* **1998**, *41*, 3872–3878. [[CrossRef](#)] [[PubMed](#)]
48. Ma, J.; Du, Z.; Xu, J.; Chu, Q.; Pang, Y. Efficient aerobic oxidation of 5-hydroxymethylfurfural to 2,5-diformylfuran, and synthesis of a fluorescent material. *ChemSusChem* **2011**, *4*, 51–54. [[CrossRef](#)] [[PubMed](#)]
49. Kalum, L.; Morant, M.D.; Lund, H.; Jensen, J.; Lapainaite, I.; Soerensen, N.H.; Pedersen, S.; Østergaard, L.H.; Xu, F. Enzymatic Oxidation of 5-Hydroxymethylfurfural and Derivatives Thereof. Google Patents WO2014015256A3, 23 January 2014.
50. Ito, N.; Phillips, S.E.; Stevens, C.; Ogel, Z.B.; McPherson, M.J.; Keen, J.N.; Yadav, K.D.; Knowles, P.F. Novel thioether bond revealed by a 1.7 Å crystal structure of galactose oxidase. *Nature* **1991**, *350*, 87–90. [[CrossRef](#)] [[PubMed](#)]
51. Chaplin, A.K.; Svistunenko, D.A.; Hough, M.A.; Wilson, M.T.; Vijgenboom, E.; Worrall, J.A. Active-site maturation and activity of the copper-radical oxidase GlxA are governed by a tryptophan residue. *Biochem. J.* **2017**, *474*, 809–825. [[CrossRef](#)] [[PubMed](#)]
52. Rogers, M.S.; Tyler, E.M.; Akyumani, N.; Kurtis, C.R.; Spooner, R.K.; Deacon, S.E.; Tamber, S.; Firbank, S.J.; Mahmoud, K.; Knowles, P.F.; et al. The stacking tryptophan of galactose oxidase: A second-coordination sphere residue that has profound effects on tyrosyl radical behavior and enzyme catalysis. *Biochemistry* **2007**, *46*, 4606–4618. [[CrossRef](#)] [[PubMed](#)]
53. Baron, A.J.; Stevens, C.; Wilmot, C.; Seneviratne, K.D.; Blakeley, V.; Dooley, D.M.; Phillips, S.E.; Knowles, P.F.; McPherson, M.J. Structure and mechanism of galactose oxidase. The free radical site. *J. Biol. Chem.* **1994**, *269*, 25095–25105. [[PubMed](#)]
54. Segato, F.; Damasio, A.R.; Goncalves, T.A.; De Lucas, R.C.; Squina, F.M.; Decker, S.R.; Prade, R.A. High-yield secretion of multiple client proteins in *Aspergillus*. *Enzym. Microb. Technol.* **2012**, *51*, 100–106. [[CrossRef](#)] [[PubMed](#)]
55. Aslanidis, C.; De Jong, P.J. Ligation-independent cloning of PCR products (LIC-PCR). *Nucleic Acids Res.* **1990**, *18*, 6069–6074. [[CrossRef](#)] [[PubMed](#)]
56. Laemmli, U.K. Cleavage of structural proteins during the assembly of the head of bacteriophage T4. *Nature* **1970**, *227*, 680–685. [[CrossRef](#)] [[PubMed](#)]
57. Perry, J.J.; Tainer, J.A. Developing advanced X-ray scattering methods combined with crystallography and computation. *Methods* **2013**, *59*, 363–371. [[CrossRef](#)] [[PubMed](#)]
58. Konarev, P.V.; Volkov, V.V.; Sokolova, A.V.; Koch, M.H.J.; Svergun, D.I. PRIMUS: A Windows PC-based system for small-angle scattering data analysis. *J. Appl. Crystallogr.* **2003**, *36*, 1277–1282. [[CrossRef](#)]
59. Svergun, D.I. Determination of the regularization parameter in indirect-transform methods using perceptual criteria. *J. Appl. Crystallogr.* **1992**, *25*, 495–503. [[CrossRef](#)]
60. Svergun, D.I. Restoring low resolution structure of biological macromolecules from solution. *Biophys. J.* **1999**, *76*, 2879–2886. [[CrossRef](#)]
61. Volkov, V.V.; Svergun, D.I. Uniqueness of ab initio shape determination in small-angle scattering. *J. Appl. Crystallogr.* **2003**, *36*, 860–864. [[CrossRef](#)]
62. Yang, J.; Yan, R.; Roy, A.; Xu, D.; Poisson, J.; Zhang, Y. The I-TASSER Suite: Protein structure and function prediction. *Nat. Methods* **2015**, *12*, 7–8. [[CrossRef](#)] [[PubMed](#)]
63. Zebisch, M.; Jackson, V.A.; Zhao, Y.; Jones, E.Y. Structure of the Dual-Mode Wnt Regulator Kremen1 and Insight into Ternary Complex Formation with LRP6 and Dickkopf. *Structure* **2016**. [[CrossRef](#)] [[PubMed](#)]
64. Pelikan, M.; Hura, G.L.; Hammel, M. Structure and flexibility within proteins as identified through small angle X-ray scattering. *Gen. Physiol. Biophys.* **2009**, *28*, 174–189. [[CrossRef](#)] [[PubMed](#)]
65. Kozin, M.B.; Svergun, D.I. Automated matching of high- and low-resolution structural models. *J. Appl. Crystallogr.* **2001**, *34*, 33–41. [[CrossRef](#)]

66. Fischer, H.; Oliveira Neto, M.D.; Napolitano, H.B.; Polikarpov, I.; Craievich, A.F. Determination of the molecular weight of proteins in solution from a single small-angle X-ray scattering measurement on a relative scale. *J. Appl. Crystallogr.* **2009**, *43*, 101–109. [[CrossRef](#)]
67. Stoll, S.; Schweiger, A. EasySpin, a comprehensive software package for spectral simulation and analysis in EPR. *J. Magn. Reson.* **2006**, *178*, 42–55. [[CrossRef](#)] [[PubMed](#)]
68. Edgar, R.C. MUSCLE: A multiple sequence alignment method with reduced time and space complexity. *BMC Bioinform.* **2004**, *5*, 113. [[CrossRef](#)] [[PubMed](#)]
69. Tamura, K.; Stecher, G.; Peterson, D.; Filipinski, A.; Kumar, S. MEGA6: Molecular Evolutionary Genetics Analysis version 6.0. *Mol. Biol. Evol.* **2013**, *30*, 2725–2729. [[CrossRef](#)] [[PubMed](#)]
70. Whittaker, J.W. Galactose oxidase. *Adv. Protein Chem.* **2002**, *60*, 1–49. [[PubMed](#)]



© 2018 by the authors. Licensee MDPI, Basel, Switzerland. This article is an open access article distributed under the terms and conditions of the Creative Commons Attribution (CC BY) license (<http://creativecommons.org/licenses/by/4.0/>).